Title	One-step direct fabrication of manganese oxide electrodes by low-temperature thermal decomposition of manganese formate-amine ink for supercapacitors
Author(s)	Yabuki, Akihiro; Matsuo, Yuki; Kang, Soonchul; Indra Wahyudhin Fathona,
Citation	Materials Science and Engineering: B , 262 : 114754
Issue Date	2020-12
DOI	10.1016/j.mseb.2020.114754
Self DOI	
URL	https://ir.lib.hiroshima-u.ac.jp/00051520
Right	© 2020. This manuscript version is made available under the CC-BY-NC-ND 4.0 license http://creativecommons.org/licenses/by-nc-nd/4.0/ This is not the published version. Please cite only the published version. この論文は出版社版ではありません。引用の際には出版社版をご確認、ご利用ください。
Relation	

One-step Direct Fabrication of Manganese Oxide Electrodes by Low-Temperature Thermal Decomposition of Manganese Formate-Amine Ink for Supercapacitors

Akihiro Yabuki,[a,*] Yuki Matsuo,[a] Soonchul Kang,[a] and Indra Wahyudhin Fathona[b]

[a] Graduate School of Engineering, Hiroshima University
1-4-1 Kagamiyama, Higashi-Hiroshima, 739-8527, Japan

[b] Engineering Physics, School of Electrical Engineering, Telkom University
Terusan Telekomunikasi, Dayeuh Kolot Bandung, 40257, Indonesia

*Corresponding author. Tel/fax: +81 82 424 7852
E-mail address: ayabuki@hiroshima-u.ac.jp (A. Yabuki)

ABSTRACT

A one-step direct fabrication of thin-film manganese oxide electrodes was accomplished via low-temperature thermal decomposition of inks composed of manganese formate (Mnf), alkylamines, and hexanol. As complexing agents, amines were used in molar ratios of Mnf:amine that ranged from 1:1 to 1:4. Prepared inks were directly coated onto the substrate, and then calcined at 170 to 210 °C under air. Cyclic voltammetry and charge/discharge measurements of the thin films were conducted in an electrolyte solution. Following immersion, the specific capacitance of the electrodes increased and eventually reached a constant value. Based on the results of cyclic voltammetry (CV) at 1 mV s^{-1}, a thin-film electrode fabricated at 180 °C from Mnf-octylamine-hexanol ink at

a molar ratio of 1:3:0.5 had the highest level of specific capacitance at 400 F g^{-1}. CV measurement at 1,000 cycles revealed a deterioration of specific capacitance of only 5%, which indicates good stability for this thin-film electrode.

Keywords: Manganese, Amine, Complex ink, Thermal decomposition, Specific capacitance

1. Introduction

Electrical energy storage devices have roles that are of paramount importance in electric vehicles and in power back-up systems such as in computers and web servers. Continuous and intensive efforts are currently underway to develop high-performance electrodes for use as supercapacitors in energy storage systems. The origin of large levels of specific capacitance in supercapacitor electrodes typically relies on two charge-storage mechanisms — an electric double layer at the electrolyte/electrode interface and the pseudocapacitive effect that electrode materials generate [1]. The enhancement of specific capacitance through the simple and low-cost fabrication of electrodes is a main objective in their development. Recent demands have included assembly for portable electronic equipment that is compact and multifunctional. These types of equipment require high flexibility, foldability, and the use of lightweight plastic as a substrate. A low-temperature fabrication process is required.

Currently, supercapacitor electrodes consisting of transition-metal oxides such as Co_3O_4 [2,3], NiO [4,5], RuO_2 [6,7], and MnOx [8,9] are being intensively investigated due to better electrical conductivity and higher capacitance. RuO_2 and MnOx are ideal materials for supercapacitors based on qualities such as good electrochemical and chemical stability, variation of oxidation states, a facile fabrication process, and high theoretical specific capacitance. RuO_2, however, is toxic, expensive, and has low porosity, which is problematic for commercialization in supercapacitors. MnOx, on the other hand, is an environmentally friendly and abundant natural resource that is non toxic while delivering high capacitance, which makes it the optimal candidate for use in supercapacitor electrodes. Electrodes of single manganese oxide have shown low specific capacitances that range from 320 to 774 F g^{-1} [10–14], although MnO_2 electrodes with a thin-film morphology have achieved a specific capacitance of 1,380 F g^{-1}, assuming the reduction MnO_2 to Mn_3O_4 as a pseudocapacitance effect for the entire portion of the thin film [15]. This effect has been achieved via a process of diffusion into the inner layer of thin films and to an enlargement of the surface area. Various fabrication methods using nanomaterials and hybrid materials have effectively enlarged the surface area of manganese oxide electrodes [8,16–25]. Research into the nano- and porous-structuring of electrodes has been reported [10–13,23,25–40]. Nanostructures of spherical particles [16,18,19,41–43], nanorods or nanowires [13,20,21,44–50], and nanosheets [51–55] have been applied to create supercapacitor electrodes. Reported examples of hybrid electrodes include reduced graphene oxide–manganese oxide (rGO-MnO_2) via a simple one-step process [56], MnO_2/graphene nanocomposites [57,58], a composite electrode of Mn_2O_3/Mn_3O_4/MnO@C fabricated by carbon coatings on manganese oxide [59], a binder-free electrospun MnO@C

nanofiber [60], an electrode of manganese zinc ferrite ($MnZnFe_2O_4$) nano-needles with a specific capacitance of 783 F g^{-1} [61], and δ-MnO_2 nanosheets as electroactive material [62]. Fabricating hybrid and composite electrodes has usually required several steps.

MnOx composite electrodes fabricated on flexible substrates are being examined for use as supercapacitors [63–66]. Murat et al. have reported that the fabrication of an electrode on carbon-fiber fabric (CFF) via a green hydrothermal method has resulted in hybrid composites of CFF and coral-like MnO_2 nanostructures with a specific capacitance of 467 F g^{-1} [63]. Carol et al. have reported the development of nanostructured carbon fiber electrodes by introducing birnessite-type potassium manganese oxide nanotubes via wet-spinning, which increased the specific capacitance to 246 F g^{-1} [64]. Yuan et al. have reported the fabrication of flexible MnO_2@carbonized cotton textile electrodes (MCCT) via a facile in-situ low-temperature chemical reaction method, which resulted in a specific capacitance of 751 F g^{-1} [65]. Huang et al. have reported a method to fabricate plain MnO_2 films for flexible transparent supercapacitors that involve arrays of MnO_2 islands deposited electrochemically on polymer films that has resulted in a specific capacitance of 4.73 mF cm^{-2}, which obviously is quite low [66]. The other important factor in flexible electrodes is the temperature constraint, because most flexible substrates are incapable of withstanding temperatures above 200 ºC.

We previously reported a single-material electrode of manganese oxide that resulted in a high level of specific capacitance [9]. That version's high specific capacitance was due to the morphology of the multi-plate thin film, which was fabricated via the thermal decomposition of manganese formate-amine ink at 260 ºC.

The thermal decomposition process used in the present proposed method features a simple one-step process that is used to fabricate copper film at temperatures ranging from 140 to 180 ºC [67–69]. The key to decreasing the temperature was the selection of suitable amines with which to prepare the ink.

In the present study, thin-film electrodes were fabricated via the thermal decomposition of manganese formate-amine ink at low temperature via a simple, one-step process. The prepared ink was spin-coated onto the substrate, and the ink was then thermally decomposed under air. Various types of amines were used and the ratio of amine to manganese formate was varied to determine the optimum conditions for thin-film electrodes. Electrochemical measurements were conducted to investigate the specific capacitance and stability of thin-film electrodes fabricated from various inks. The morphology and microstructure of this thin-film electrode was observed and analyzed.

2. Experimental

2.1. Preparing an ink of manganese formate-amine

Powder of manganese (II) formate dihydrate was used as a manganese source. The powder was heated at 160 ºC under vacuum conditions for 1 h to obtain anhydrous manganese formate (Mnf), which was then mixed with amine and hexanol. Heptylamine (bp: 155 ºC), octylamine (bp: 176 ºC), and nonylamine (bp: 201 ºC) were used as complexing agents, and were purchased from Wako Chemical, Ltd., Japan. Hexanol (bp: 157 ºC) was added to adjust the viscosity of the ink. The molar ratios

(Mnf:amine:hexanol) were varied at 1:1:1, 1:2:0.5, 1:3:0.5, and 1:4:0.5. The mixed ink was thoroughly kneaded with a spatula to incorporate the manganese-amine complex.

Thermal gravimetric (TG) analyses of the Mnf-amine-hexanol ink complexes were conducted using a thermal gravimetric analyzer (TG-DTA 6300, EXSTAR6000, SII Nano Technology Inc., Japan) at a heating rate of 5 ^{o}C min^{-1} under an air atmosphere.

2.2. Fabrication of thin-film electrodes

The ink mixture was coated onto a stainless steel substrate (10 x 10 mm) [12, 22], and adhesive tape with a 5 mm hole in the diameter was attached. The coating was conducted using a spin coater (1H-DX II, Mikasa Co. Ltd., Japan) at rotating speeds of 3,000 to 5,000 rpm for 1 min to control the mass loading of the thin-film electrodes. The substrate-coated ink was calcined on a hot plate (HP 2SA, As One Co., Japan) by heating from room temperature at heating rate 5 ^{o}C min^{-1} for 40 min under an air atmosphere to reach setting temperatures ranging from 170 to 210 ^{o}C. An electronic balance (CP225D, Sartorius AG Co., Germany) was used to measure the difference between the mass of a plain substrate and that of a substrate with the active material after calcination. The mass loading of the thin-film electrodes ranged from 0.1 to 0.2 mg. The thickness of the electrode was approximately 0.1 to 0.2 μm.

The morphologies of the thin-film electrodes fabricated under various conditions were observed using a scanning electron microscope (SEM, VE-7800, Keyence Corp., Japan). An X-ray diffractometer (XRD MiniFlex600, Rigaku Co. Ltd.) with Cu Kα monochromatized radiation was used to analyze the structures of the thin-film electrodes.

2.3. Electrochemical measurement

A three-electrode system that involved a potentio/galvanostat (Compact Stat, Ivium Technologies) was used for the electrochemical testing of the thin-film electrodes, which was conducted under 0.5 M of Na_2SO_4 electrolyte-purged nitrogen gas at 35 ºC. An Ag/AgCl electrode in saturated KCl solution and a platinum plate served as the reference and counter electrodes, respectively. Cyclic voltammetry (CV) was measured over a potential of 0 to 1.0 V vs. the Ag/AgCl with scan rates of 1 to 100 mV s^{-1} during 20 to 1,000 cycles. Galvanostatic charge/discharge (CD) was measured for a potential that ranged from 0 to 0.9 V vs. Ag/AgCl with a current of 1 to 10 mA. The stability of the thin-film electrodes was evaluated via CV measurement for 1,000 cycles.

The specific capacitance of the thin-film electrodes was calculated by integrating the CV curves with respect to the potential window as described in Eq. (1), where m is the mass loading, ΔV is the potential window, and v is the scan rate.

$$C = \frac{1}{m\Delta V v}\int_{V_i}^{V_f} I\, dV \tag{1}$$

By comparison, the specific capacitances of the thin-film electrodes were also calculated from a chronopotentiogram of the CD data using Eq. (2).

$$C = \frac{I}{(\Delta E/\Delta t)m} \tag{2}$$

In Eq. 2, I is the current and $\Delta E/\Delta t$ is the slope of the discharge curve at potential ΔE with a discharge time of Δt. Therefore, the specific capacitance (gravimetric capacitance, F g^{-1}), or real capacitance (F), can be calculated using Eqs. 1 and 2. The

specific capacitance was calculated by dividing the real capacitance by the initial mass of the active material measured following the calcination process.

3. Results and discussion

3.1. Properties of manganese formate-amine ink

The TG analyses of Mnf powder and Mnf-amine-hexanol inks with various types of amines at the prescribed molar ratio (Mnf:amine:hexanol = 1:2:0.5) under air are shown in Fig. 1. A significant mass decrease in Mnf powder was observed at 230-260 ºC, followed by a constant value of 53% as the temperature increased (Fig. 1a). The mass decrease was due to the thermal decomposition of Mnf and to the oxidation to manganese oxide under air [9]. The masses of Mnf-heptylamine-, Mnf-octylamine-, and Mnf-nonylamine-hexanol inks were gradually decreased at several steps to a range of from 20-200 ºC. This showed that the thermal decomposition of Mnf was decreased by the addition of amines, but the decomposition process was different. The temperatures for the three steps differed according to the type of amine at 20-150, 60-170, and 60-200 ºC for Mnf-heptylamine-, Mnf-octylamine- and Mnf-nonylamine-hexanol inks, respectively. The decomposition temperature corresponded to the boiling point of each amine, and ink with an amine that had a lower boiling point showed a lower decomposition temperature. This allowed for large decreases in temperatures that were lower than the boiling point of each amine (heptylamine: 155 ºC, octylamine: 176 ºC, nonylamine: 201 ºC), because the temperature of total decomposition approximated the boiling point. The final product calcined from the inks using amine and after

electrochemical measurement was Mn_3O_4 as indicated by XRD data in a following section. The amount of Mnf as a source of manganese in the Mnf-heptylamine-hexanol ink was 34.0 wt%. When the thermal decomposition and oxidation had finished, and the Mnf was transformed to Mn_3O_4 under air, the mass percentage of Mn_3O_4 was 47.2 wt% (=34.0 x 229/(3 x 55)), when using Mn at 55 g mol^{-1}, and Mn_3O_4 at 229 g mol^{-1}. According to the TG data, the remaining mass following the thermal decomposition of Mnf-heptylamine-hexanol ink was approximately 55 wt%, which resulted in a larger mass following calcination. This showed that Mnf remains in the products, as shown later. The same calculation for Mnf-octylamine- and Mnf-nonylamine-hexanol ink showed that Mnf remained in the products, although the temperature of thermal decomposition was decreased.

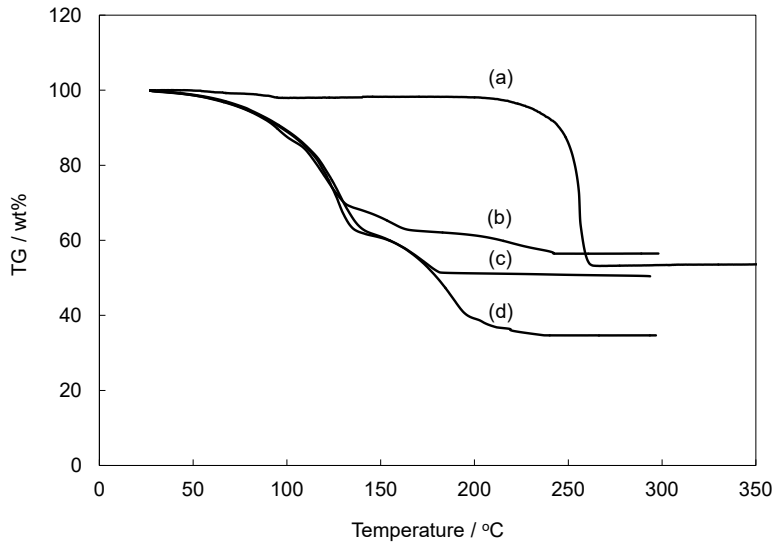

Fig.1. Thermal gravimetric analysis of (a) Mnf, (b) Mnf-heptylamine-hexanol, (c) Mnf-octylamine-hexanol, and (d) Mnf-nonylamine-hexanol inks under air. The molar ratio of Mnf:amine:hexanol was 1:2:0.5.

3.2. Electrochemical performance of thin-film electrodes

The CV curve of a thin-film electrode fabricated at 180 ºC from Mnf-amine-hexanol using various types of amines with a scan rate of 50 mV s^{-1} is shown in Fig. 2. The molar ratio of Mnf-amine-hexanol was 1:2:0.5. An almost semi-rectangular shape was observed in all samples. The manganese oxide electrode that was fabricated showed a semi-rectangular shape CV, which is typical of a pseudocapacitive oxide, although some of the peaks on the CV curve were of metal oxide composite materials [70]. The electrode fabricated from Mnf-octylamine-hexanol ink showed wavy portions in a potential range of 0.4 to 0.8 V, which indicated a reversible redox reaction had occurred on the surface of the thin-film electrode [70]. The specific capacitances of each of the thin-film electrodes were calculated using Eq. (1) in order to compare the properties.

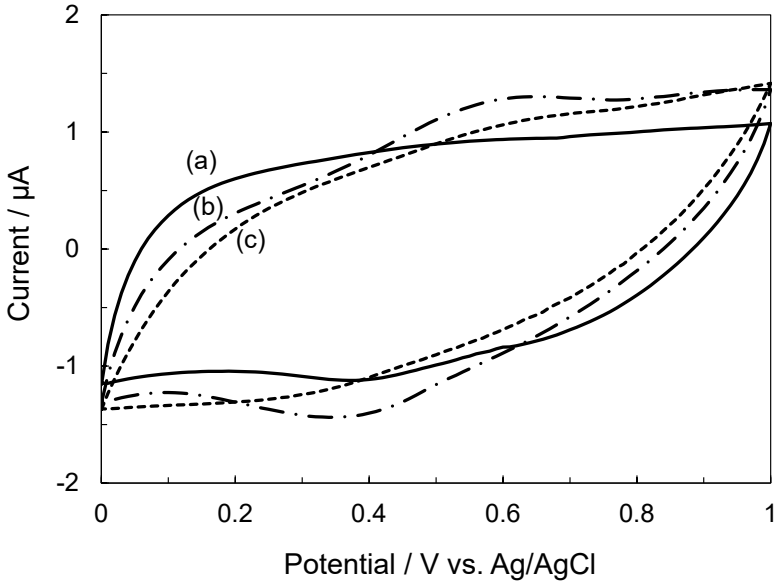

Fig. 2. Cyclic voltammetry of a thin-film electrode fabricated at 180 ºC from (a) Mnf-heptylamine-hexanol, (b) Mnf-octylamine-hexanol, and (c) Mnf-nonylamine-hexanol inks. The molar ratio of Mnf:amine:hexanol is 1:2:0.5. The scan rate was 50 mV s^{-1}.

The specific capacitances calculated from the CV curves of thin-film electrodes fabricated at 180 ºC for various Mnf-amine-hexanol inks (molar ratio is 1:2:0.5) is shown in Fig. 3. The scan rate was 50 mV s^{-1}. The specific capacitance of each thin-film electrode showed low values of 12 to 70 F g^{-1} at the initial measurement, but a gradual increase resulted in a constant-value state after 30 cycles. In a comparison of the specific capacitance of each electrode after 50 cycles, the thin-film electrode fabricated from Mnf-octylamine-hexanol ink showed the highest value at 100 F g^{-1}.

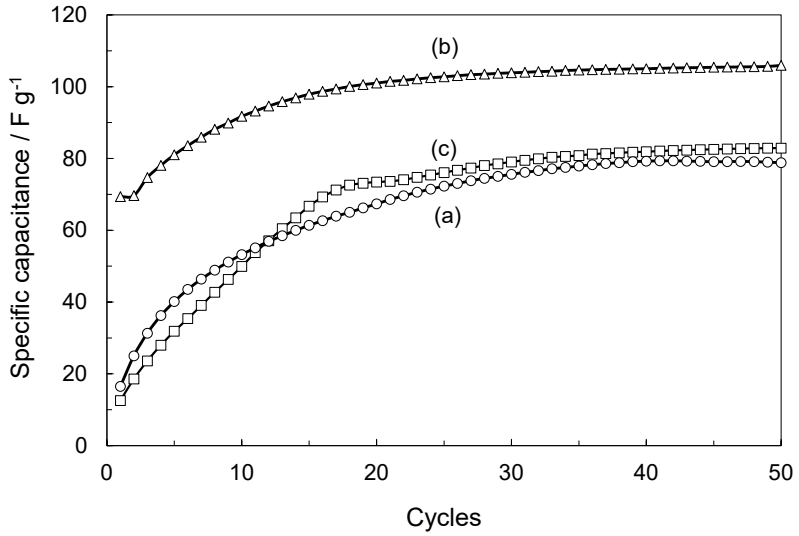

Fig. 3. Specific capacitance calculated from CV curves of thin-film electrodes fabricated at 180 ºC from (a) Mnf-heptylamine-hexanol, (b) Mnf-octylamine-hexanol, and (c) Mnf-nonylamine-hexanol inks. The molar ratio of Mnf:amine:hexanol was 1:2:0.5. The scan rate was 50 mV s^{-1}.

Fig. 4 shows the CV curve of a thin-film electrode fabricated at 180 ºC from Mnf-octylamine-hexanol inks with various ratios of Mnf:octylamine. Semi-rectangular shapes were observed in all samples, although wavy portions in a potential range of 0.4 to 0.8 V were observed in the samples with ratios of 1:1, 1:2, and 1:3. Fig. 5 shows the calculations for specific capacitance based on the CV of thin-film electrodes fabricated

at 180 ºC from Mnf-octylamine-hexanol inks for various molar ratios. The scan rate was 50 mV s^{-1}. The specific capacitance of each thin-film electrode fabricated from Mnf-octylamine-hexanol ink showed a similar behaviour of increases before reaching an almost constant value, as shown in Fig. 5. The specific capacitance of the electrodes fabricated from inks with Mnf:amine ratios of 1:1 and 1:4 showed the same values after the first measurement (Fig. 5ad), whereas the specific capacitance of the electrodes fabricated from inks with Mnf:amine ratios of 1:2 and 1:3 (Fig. 5bc) showed the same, or higher, values than the electrodes with ratios of 1:1 and 1:4. CV measurement showed a large increase in specific capacitance of electrodes fabricated from inks with a ratio of 1:3 after 20 cycles, and then a gradual increased of up to 50 cycles. Measurements of specific capacitance after 50 cycles showed 24, 105, 325, and 73 F g^{-1} for Mnf:amine ratios of 1:1, 1:2, 1:3 and 1:4, respectively. Thus, the specific capacitance was the maximum at an Mnf:amine ratio of 1:3.

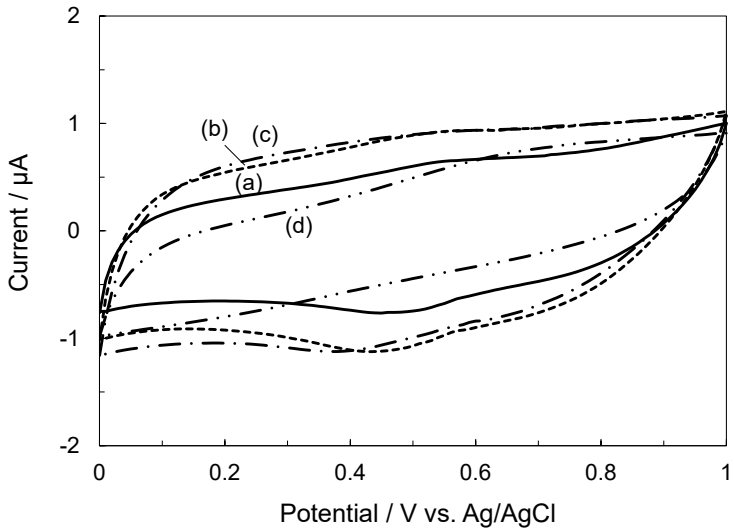

Fig. 4. CV curves of the thin-film electrodes fabricated at 180 ºC from Mnf-octylamine-hexanol inks with Mnf:octylamine ratios of (a) 1:1, (b) 1:2, (c) 1:3, and (d) 1:4. The scan rate was 50 mV s^{-1}.

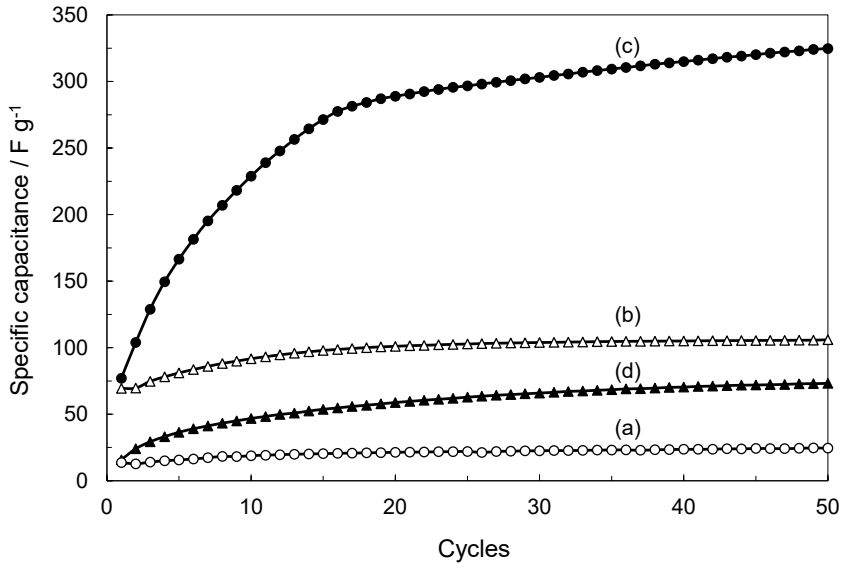

Fig. 5. Specific capacitance calculated from the CV curves of the thin-film electrodes fabricated at 180 ºC from Mnf-octylamine-hexanol inks with Mnf:octylamine ratios of (a) 1:1, (b) 1:2, (c) 1:3, and (d) 1:4. The scan rate was 50 mV s^{-1}.

Fig. 6 shows the specific capacitance calculated from the measurement of CV curves after 50 cycles for thin-film electrodes fabricated from Mnf-octylamine-hexanol inks with various Mnf-octylamine ratios at various temperatures. The scan rate was 50 mV s^{-1}. The specific capacitance for a ratio of 1:1 increased from 59 to 211 F g^{-1} as the temperature increased from 170 to 210 ºC, for which the high specific capacitance was observed at 210 ºC (Fig. 6a). The specific capacitance reached the maximum at a certain temperature, which differed for molar ratios of 1:2, 1:3, and 1:4, and the maximum specific capacitances of thin-film electrodes were 283 F g^{-1} at 200 ºC (ratio of 1:2, Fig. 6b), 325 F g^{-1} at 180 ºC (ratio of 1:3, Fig. 6c), and 192 F g^{-1} at 190 ºC (ratio of 1:4, Fig. 6d). This was caused by the surface morphology of the thin films, as shown later. These results showed that the thin-film electrode with the highest specific capacitance was obtained via calcination of Mnf-octylamine-hexanol ink with an Mnf:amine ratio of 1:3

at 180 ºC. Thus, the calcination temperature to fabricate a thin-film electrode using octylamine was achieved at 180 °C, which is significantly lower than the temperature of 260 °C that is required for the fabrication of a thin-film electrode using TETA (Triethylenetetramine) [9]. Such a low temperature would allow application to a flexible substrate. The decrease in calcination temperature was related to the boiling point of octylamine, 176 °C, which approximates calcination temperature, because the synthesis of manganese oxide electrodes proceeds in solution.

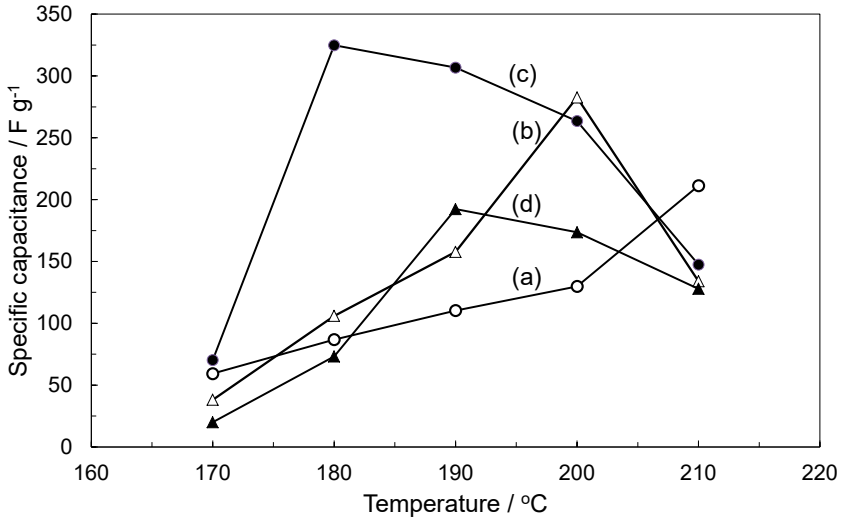

Fig. 6. Specific capacitance calculated from the CV curves after 50 cycles for a thin-film electrode fabricated from Mnf-octylamine-hexanol ink with Mnf:octylamine ratios of (a) 1:1, (b) 1:2, (c) 1:3, and (d) 1:4 at various temperatures. The scan rate was 50 mV s^{-1}.

The effect of the scan rate on the thin-film electrode was investigated to confirm the properties of pseudocapacitance. Fig. 7 shows the specific capacitances measured at scan rates that ranged from 1 to 100 mV s^{-1}. The specific capacitance was approximately 300 F g^{-1} at a scan rate of 30 to 100 mV s^{-1}. On the other hand, the specific capacitance was increased when the scan rate was low, which resulted in a

value of 400 F g^{-1}. The low specific capacitance was the result of an insufficient diffusion of ions into the inner layer of the electrode [71]. As the scan rate was changed from 50 to 10 mV s^{-1}, the ratio of specific capacitance increased to 20%. This suggested a large amount of diffusion into a relatively thick inner layer. Thus, the fabricated thin-film electrode projected pseudocapacitive properties.

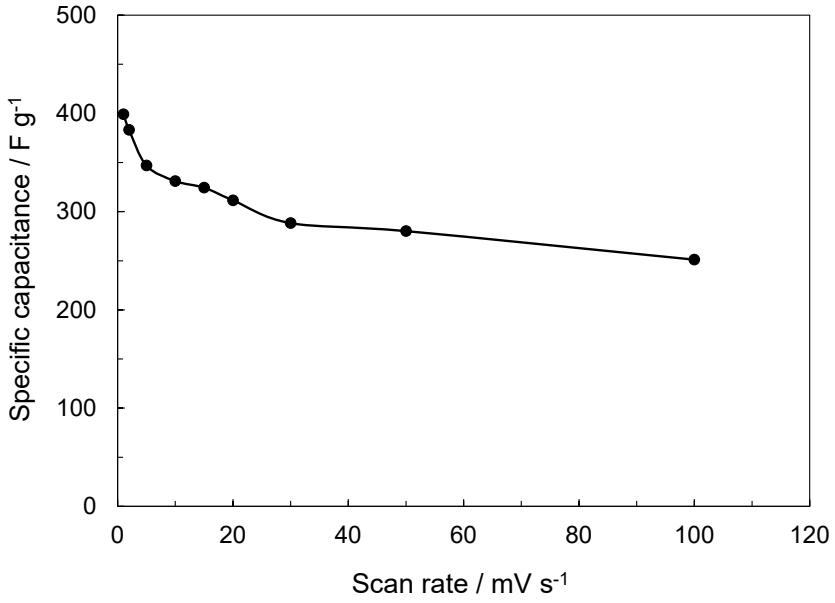

Fig. 7. Specific capacitance calculated from the CV curves after 50 cycles of a thin-film electrode fabricated from Mnf-octylamine-hexanol ink with a Mnf:octylamine ratio of 1:3 at various scan rates.

Fig. 8 shows 48-50 cycles of charge-discharge (CD) curves for a thin-film electrode fabricated at 180 ºC from Mnf-octylamine-hexanol ink with a Mnf:amine molar ratio of 1:3 at 1 and 10 mA. The CD curves show a linear trend and symmetric behavior. The specific capacitances calculated from the 48 to 50 cycles using Eq. 2 were almost constant at 312 and 216 F g^{-1} for 1 and 10 mA, respectively. The specific capacitance was similar to that obtained from CV measurement, as shown in Fig. 7. The small

dissimilarities in the values for specific capacitance calculated from CD and CV were due to the differences in the range of potential.

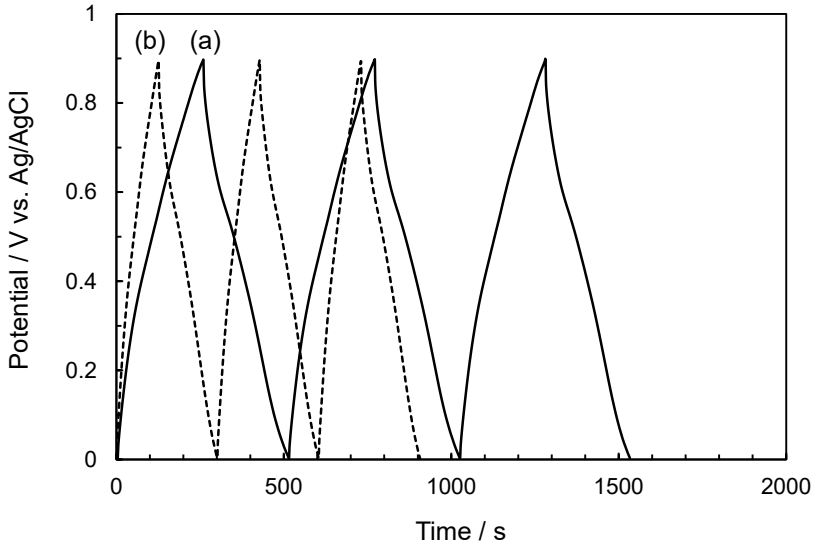

Fig. 8. Charge-discharge curves during 48 to 50 cycles of thin-film electrodes fabricated at 180 ºC from Mnf-octylamine-hexanol ink with a Mnf:amine ratio of 1:3 at 1 mA (a) and 10 mA (b).

Next, we measured the electrochemical impedance spectroscopy (EIS) of the thin-film electrode fabricated at 180 ºC from Mnf-octylamine-hexanol ink with a Mnf:amine molar ratio of 1:3. Fig. 9 shows a Nyquist plot of the thin-film electrode at 0.6 V vs. Ag/AgCl in an electrolyte solution. At the high frequency of a sine wave, the intercept between the initial value in the semicircle and the x-axis is considered an equivalent series of the thin film that would be contact resistant, electrolyte resistant, and internal resistant, and resulted in a value of 2 Ω cm^2 (right figure in Fig. 9). The resistance of charge transfer generated by the faradaic reaction on the surface of the thin film was calculated from the diameter of the semicircle curve (dotted line in right figure) that resulted in a value of 4 Ω cm^2. The linear, sharply increasing line in the low-frequency

region displays the Warburg resistance and indicates fast speeds of diffusion and adsorption of ions onto the electrode surface [72–75]. This result confirmed the dominance of the capacitive properties during the formation of the charge storage on the electrode surface [72–75]. That result is in good agreement with the corresponding specific capacitance data. Therefore, the high specific capacitance of the thin-film electrode fabricated at 180 ºC from Mnf-octylamine-hexanol ink with a Mnf:amine molar ratio of 1:3 was confirmed by EIS and both CV and CD measurement.

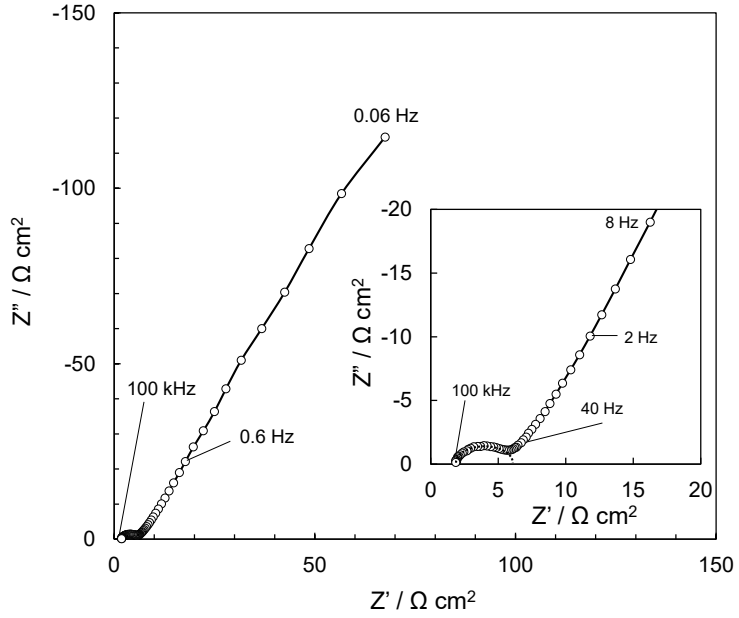

Fig. 9. Nyquist plot of a thin-film electrode fabricated at 180 ºC from Mnf-octylamine-hexanol ink with a Mnf:amine ratio of 1:3.

CV measurements were conducted for 1,000 cycles to evaluate the performance and stability of these thin-film electrodes. Fig. 10 shows the specific capacitance calculated from the CV curves during 1,000 cycles of the thin-film electrodes of ink complexes fabricated at 180 ºC from Mnf-octylamine-hexanol ink with a Mnf:amine molar ratio of 1:3. The specific capacitance of these thin-film electrodes was increased and remained

constant after approximately 50 cycles of CV measurement. After 1,000 cycles, the specific capacitance of the thin-film electrodes had decreased by only 2% from each of the maximum values. The decreases in specific capacitance in the thin-film electrodes were low. Thus, the thin-film electrodes fabricated at 180 ºC from Mnf-octylamine-hexanol ink with a Mnf:amine molar ratio of 1:3 showed good stability.

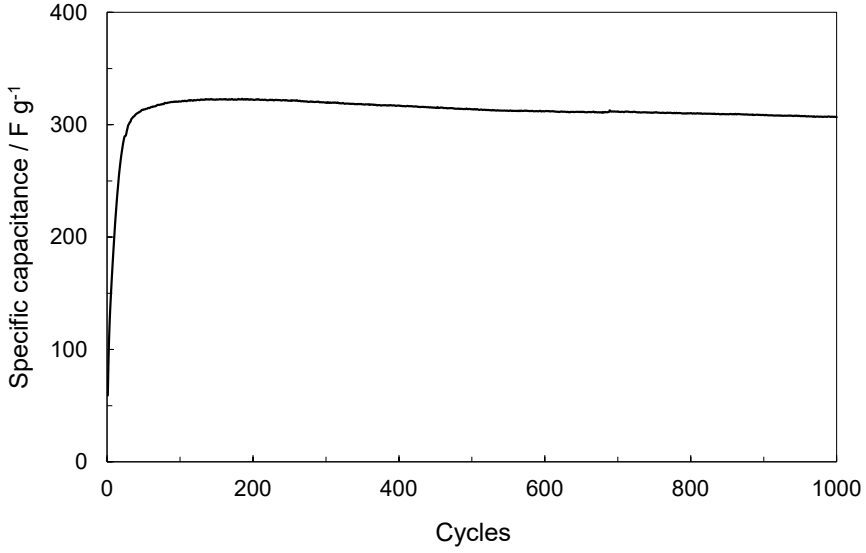

Fig. 10. Specific capacitances of thin-film electrodes fabricated from Mnf-octylamine-hexanol ink with Mnf:amine molar ratios of 1:3 at 180 ºC calculated from CV during 1,000 cycles at a scan rate 50 mV s^{-1}.

3.3. Morphology of thin-film electrodes

The surface morphologies of thin-film electrodes fabricated at 180 ºC from Mnf-octylamine-hexanol ink with various Mnf:octylamine molar ratios after 50 cycles of CV measurement are shown in Fig. 11. The thin-film electrode with a molar ratio of 1:2 consisted of large particles with gap-like cracks of 0.5 μm (Fig. 11a). The thin-film electrode with a molar ratio of 1:3 showed small gaps between protrusions of 0.5 μm,

but no cracks (Fig. 11b). The thin-film electrode with a molar ratio of 1:4 indicated many gaps of 0.5 μm between pillars (Fig. 11c). The specific capacitance of the thin-film electrode with a molar ratio of 1:3 was four-fold larger than that of the thin-film electrodes with molar ratios of 1:2 and 1:4, as shown in Fig. 6.

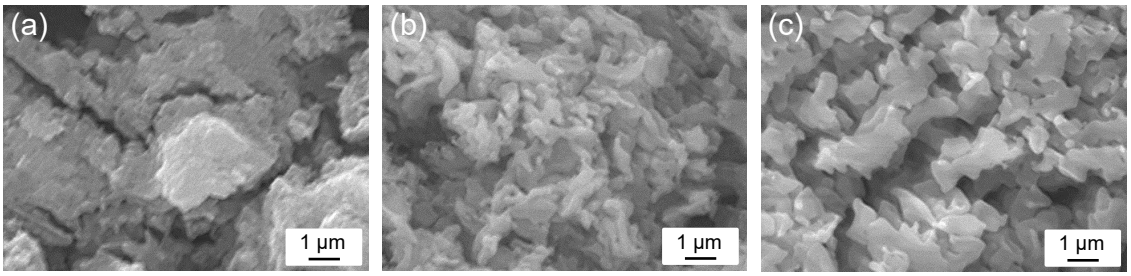

Fig. 11. Surface morphology of thin films fabricated at 180 ºC from Mnf-octylamine-hexanol ink with Mnf:amine ratios of (a) 1:2, (b) 1:3, and (c) 1:4 after 50 cycles of CV measurement with a scan rate of 50 mV s^{-1}.

Fig. 12 shows the effect that 50 cycles exerted on the surface morphologies of thin-film electrodes fabricated at 170 and 210 ºC from Mnf-octylamine-hexanol ink with a Mnf:amine molar ratio of 1:3. Compared with the results at 180 ºC (Fig. 11b), the surfaces of the thin-film electrodes fabricated at 170 and 210 ºC were smooth and protrusions were not observed, although no gaps were observed, as shown in Fig. 11b. The smooth surface of thin film fabricated at 170 ºC due to the formation of manganese oxide particles was not in the final process of thermal decomposition, as shown in the decline curve in the TG results (Fig. 1c); thus, manganese oxide particles were not generated to form protrusion as with a temperature of 180 ºC. At a temperature of 210 ºC the manganese oxide was in the final process of thermal decomposition, as shown by the flat TG curve (Fig. 1c), which resulted in a compact arrangement of manganese

oxide particles on the thin film surface. A calcination temperature of 180 ºC approximated the boiling point of octylamine (bp: 176 ºC), and the manganese oxide grew in the solvent during evaporation and generated 0.5 μm protrusions (Fig. 11b). The thin-film electrodes with small protrusions, but no gaps, had a higher level of specific capacitance.

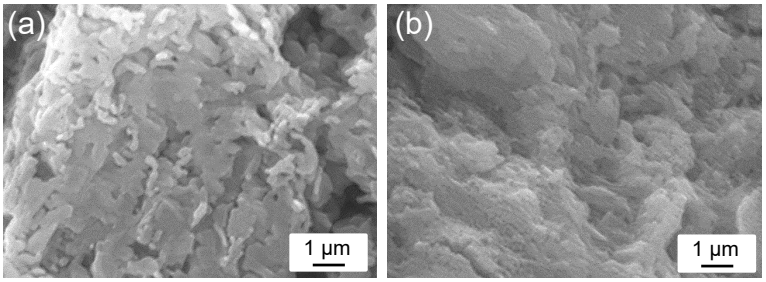

Fig. 12. Surface morphology of thin films fabricated at (a) 170 ºC, and (b) 210 ºC from Mnf-octylamine-hexanol ink with a Mnf:amine ratio of 1:3 after 50 cycles of CV measurement with a scan rate of 50 mV s^{-1}.

The surface morphology of thin films fabricated at 180 ºC from Mnf-octylamine-hexanol ink with a Mnf:amine ratio of 1:3 before electrochemical measurement is shown in Fig. 13. Compared with the surfaces following electrochemical measurement (Fig. 11b), the morphology was relatively smooth with no protrusions. This was caused by the dissolution of the unreacted Mnf that remained during electrochemical measurement, as previously reported [76]. The low specific capacitance at the initial measurement of thin-film electrodes (Figs. 3, 4 and 9) was due to the dissolution of Mnf, although the behavior of each thin film was different.

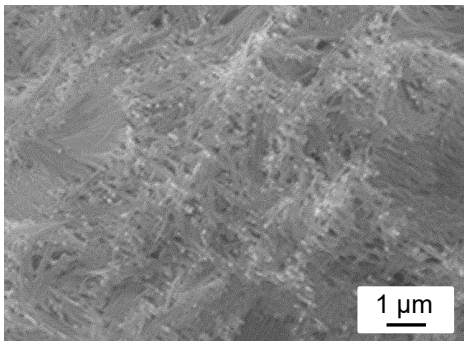

Fig. 13. Surface morphology of a thin film fabricated at 180 ºC from Mnf-octylamine-hexanol ink with a Mnf:amine ratio of 1:3 before electrochemical measurement.

The XRD peaks of the thin-film electrode calcined at 180 ºC with a Mnf:amine molar ratio of 1:3 before and after immersion in an electrolyte solution are shown in Fig. 14ab. For comparison, the XRD peaks of a thin-film electrode calcined at 180 ºC with a Mnf:amine molar ratio of 1:2 before immersion in an electrolyte solution appear in Fig. 14c. The XRD of the thin film before immersion showed peaks similar to those of Mnf and Mn_3O_4, which were the result of Mnf that remained in the thin film (Fig. 14a). On the other hand, the XRD of the thin film following immersion in the electrolyte solution also showed several peaks that matched the characteristic peak of Mn_3O_4 at angles of 18.4º, 29.04º, 32.53º, 39.15º, 55º, 57.69º, and 74º (JP JCPDS 18-0803/ICSD-68174) (Fig. 14b). This shows that the remaining Mnf was dissolved by the immersion in an electrolyte solution. Observation of the thin film before and after electrochemical measurement agreed with this observation (Figs. 11b and 13). Before immersion in the electrolyte solution, the peaks of Mnf for the electrode calcined with a Mnf:amine molar ratio of 1:3 were lower than those from an electrode with a molar ratio of 1:2 (Fig. 14c), which confirmed the superior reactivity of the 1:3 version.

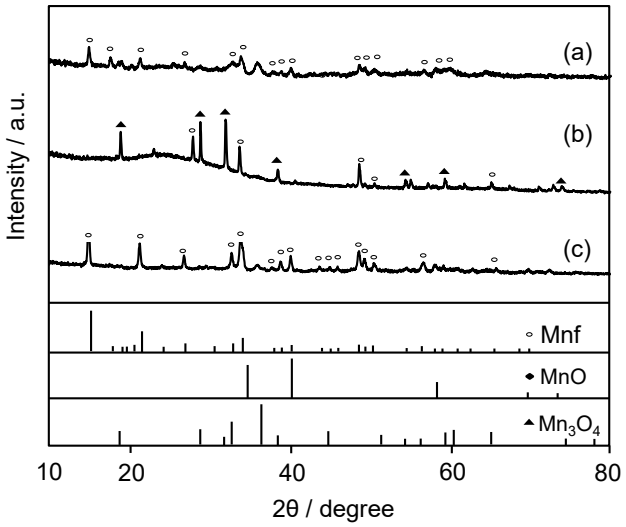

Fig. 14. XRD pattern of thin-film electrodes fabricated at 180 ºC from Mnf-octylamine-hexanol ink with a Mnf:amine molar ratio of 1:3 (a) before and (b) after immersion in an electrolyte solution, and ink with a ratio of 1:2 before immersion in electrolyte (c).

The thin-film electrode from Mnf and octylamine ink with a ratio of 1:3 developed in this study was generated in two stages, as shown in Fig. 15.

(1) In the first stage, the formation of manganese oxide and growth occurs via thermal decomposition of the Mnf-amine complex. Growth is an important process that is stopped mid-process by evaporation of the solvent, which results in a remaining portion of unreacted Mnf. As indicated by XRD, a smaller amount of Mnf remained in the 1:3 film than that in the 1:2 version. This shows that the excess amine acts as a solvent, because a calcination temperature of 180 ºC approximates the boiling point of octylamine (bp: 176 ºC). As a result, the manganese oxide grows in the solvent and generates 0.5 μm protrusions (Fig. 11b). The growth of manganese oxide in the ink of the 1:2 version was insufficient, and resulted in a smooth surface. In the ink of the 1:4 version, the protrusion of manganese oxide grew larger, due to the increased length of

the reaction. Hexanol also acted as a solvent, and it also was related to the growth of manganese oxide.

(2) In the second stage, the remainder of the Mnf in the thin-film electrode was gradually dissolved during electrochemical measurement in the electrolyte solution, which resulted in growth of the manganese oxide protrusions and exposure to the electrolyte solution wherein many ions were adsorbed onto the increased active surface area of the protruding morphology leading to the generation of a high degree of electrochemical capacitance.

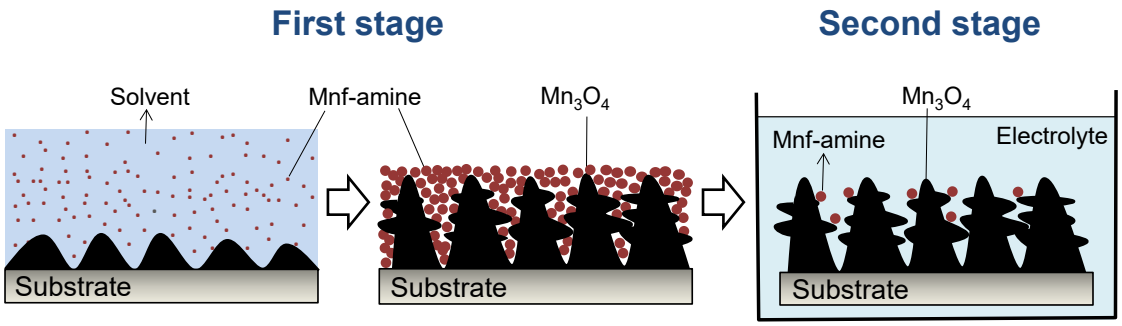

Fig.15. Mechanism of the formation and growth of a thin-film electrode with high specific capacitance through calcination and electrochemical measurement in an electrolyte solution to generate an electrochemically active surface.

4. Conclusions

Thin-film electrodes intended for use as supercapacitors were fabricated via the thermal decomposition of manganese formate-amine ink at low temperature in a simple, one-step process. The prepared ink was coated onto a substrate via a spin coater, and was then calcined under air. Various amines were tested to determine the optimum low temperature of calcination that would result in thin-film electrodes with a high level of

specific capacitance. The molar ratio of Mnf:octylamine in inks and the calcination temperatures were varied, which revealed a ratio of 1:3 was the optimum at a temperature of 180 ^{o}C. The specific capacitance was increased after immersion and reached a constant value. The thin-film electrode fabricated at 180 ^{o}C from Mnf-octylamine-hexanol ink with the optimum molar ratio showed a high specific capacitance of 400 F g^{-1} at a CV measurement of 1 mV s^{-1}. The protruding morphology had a large area that could adsorb many ions and resulted in a high level of specific capacitance. Following 1,000 cycles of CV measurement, specific capacitance had deteriorated by only 5%, which indicates good stability for this thin-film electrode. This electrode was fabricated by low temperature thermal decomposition of Mnf-based ink via one-step and it is expected to have applications on flexible substrates.

Data Availability statement: Data will be made available on request.

This research received no specific grants from any funding agencies in the public, commercial, or not-for-profit sectors.

Conflicts of interest: none.

References

[1] J.R. Miller, P. Simon, Fundamentals of electrochemical capacitor design and operation, Electrochem. Soc. Interface. 17 (2008) 31.

[2] Y. Xiao, A. Dai, X. Zhao, S. Wu, D. Su, X. Wang, S. Fang, A comparative study of one-dimensional and two-dimensional porous CoO nanomaterials for asymmetric supercapacitor, J. Alloys Compd. 781 (2019) 1006–1012.

https://doi.org/https://doi.org/10.1016/j.jallcom.2018.12.129.

[3] N. Tang, W. Wang, H. You, Z. Zhai, J. Hilario, L. Zeng, L. Zhang, Morphology tuning of porous CoO nanowall towards enhanced electrochemical performance as supercapacitors electrodes, Catal. Today. 330 (2019) 240–245. https://doi.org/https://doi.org/10.1016/j.cattod.2018.03.024.

[4] X. Feng, Y. Huang, C. Li, X. Chen, S. Zhou, X. Gao, C. Chen, Controllable synthesis of porous $NiCo_2O_4$/NiO/Co_3O_4 nanoflowers for asymmetric all-solid-state supercapacitors, Chem. Eng. J. 368 (2019) 51–60. https://doi.org/https://doi.org/10.1016/j.cej.2019.02.191.

[5] P. Liu, M. Yang, S. Zhou, Y. Huang, Y. Zhu, Hierarchical shell-core structures of concave spherical NiO nanospines@carbon for high performance supercapacitor electrodes, Electrochim. Acta. 294 (2019) 383–390. https://doi.org/https://doi.org/10.1016/j.electacta.2018.10.112.

[6] T.N. Jebakumar Immanuel Edison, R. Atchudan, Y.R. Lee, Facile synthesis of carbon encapsulated RuO_2 nanorods for supercapacitor and electrocatalytic hydrogen evolution reaction, Int. J. Hydrogen Energy. 44 (2019) 2323–2329. https://doi.org/https://doi.org/10.1016/j.ijhydene.2018.02.018.

[7] D. Zhu, Q. Zhou, A. Liang, W. Zhou, Y. Chang, D. Li, J. Wu, G. Ye, J. Xu, Y. Ren, Two-step preparation of carbon nanotubes/RuO_2/polyindole ternary nanocomposites and their application as high-performance supercapacitors, Front. Mater. Sci. 14 (2020) 109–119. https://doi.org/10.1007/s11706-020-0497-5.

[8] Z. Sun, Y. Zhang, Y. Liu, J. Fu, S. Cheng, P. Cui, E. Xie, New insight on the mechanism of electrochemical cycling effects in MnO_2-based aqueous supercapacitor, J. Power Sources. 436 (2019) 226795.

https://doi.org/https://doi.org/10.1016/j.jpowsour.2019.226795.

[9] I.W. Fathona, A. Yabuki, Multi-plate, thin-film electrodes of manganese oxide synthesized via the thermal decomposition of a manganese-amine complex for use as electrochemical supercapacitors, Electrochim. Acta. 222 (2016). https://doi.org/http://dx.doi.org/10.1016/j.electacta.2016.11.025.

[10] N. Nagarajan, H. Humadi, I. Zhitomirsky, Cathodic electrodeposition of MnOx films for electrochemical supercapacitors, Electrochim. Acta. 51 (2006) 3039–3045. https://doi.org/10.1016/j.electacta.2005.08.042.

[11] J. Li, I. Zhitomirsky, Cathodic electrophoretic deposition of manganese dioxide films, Colloids Surfaces A Physicochem. Eng. Asp. 348 (2009) 248–253. https://doi.org/10.1016/j.colsurfa.2009.07.035.

[12] N. Nagarajan, M. Cheong, I. Zhitomirsky, Electrochemical capacitance of MnOx films, Mater. Chem. Phys. 103 (2007) 47–53. https://doi.org/10.1016/j.matchemphys.2007.01.005.

[13] H. Xia, J. Feng, H. Wang, M.O. Lai, L. Lu, MnO_2 nanotube and nanowire arrays by electrochemical deposition for supercapacitors, J. Power Sources. 195 (2010) 4410–4413. https://doi.org/10.1016/j.jpowsour.2010.01.075.

[14] S. Shi, C. Xu, C. Yang, Y. Chen, J. Liu, F. Kang, Flexible asymmetric supercapacitors based on ultrathin two-dimensional nanosheets with outstanding electrochemical performance and aesthetic property., Sci. Rep. 3 (2013) 2598. https://doi.org/10.1038/srep02598.

[15] M. Toupin, T. Brousse, D. Bélanger, Charge Storage Mechanism for MnO_2 Electrode Used in Aqueous Electrolyte electrochemical capacitor, Si. (2004) 2–5. http://pubs.acs.org/doi/abs/10.1021/cm049649j.

[16] B. You, J. Yang, Y.Q. Sun, Q.D. Su, Easy synthesis of hollow core, bimodal mesoporous shell carbon nanospheres and their application in supercapacitor, Chem. Commun. 47 (2011) 12364–12366. https://doi.org/Doi 10.1039/C1cc15348j.

[17] C. Zhou, Y. Zhang, Y. Li, J. Liu, Construction of High-Capacitance 3D CoO@Polypyrrole Nanowire Array Electrode for Aqueous Asymmetric Supercapacitor, Nano Lett. 13 (2013) 2078–2085. https://doi.org/10.1021/nl400378j.

[18] Z. Yang, F. Xu, W. Zhang, Z. Mei, B. Pei, X. Zhu, Controllable preparation of multishelled NiO hollow nanospheres via layer-by-layer self-assembly for supercapacitor application, J. Power Sources. 246 (2014) 24–31. https://doi.org/10.1016/j.jpowsour.2013.07.057.

[19] Z. Lei, Z. Chen, X.S. Zhao, Growth of polyaniline on hollow carbon spheres for enhancing electrocapacitance, J. Phys. Chem. C. 114 (2010) 19867–19874. https://doi.org/10.1021/jp1084026.

[20] G.Q. Zhang, H. Bin Wu, H.E. Hoster, M.B. Chan-Park, X.W. (David) Lou, Single-crystalline $NiCo_2O_4$ nanoneedle arrays grown on conductive substrates as binder-free electrodes for high-performance supercapacitors, Energy Environ. Sci. 5 (2012) 9453. https://doi.org/10.1039/c2ee22572g.

[21] Q. Qu, Y. Zhu, X. Gao, Y. Wu, Core-shell structure of polypyrrole grown on V_2O_5 nanoribbon as high performance anode material for supercapacitors, Adv. Energy Mater. 2 (2012) 950–955. https://doi.org/10.1002/aenm.201200088.

[22] Z. Yu, L. Tetard, L. Zhai, J. Thomas, Supercapacitor electrode materials: nanostructures from 0 to 3 dimensions, Energy Environ. Sci. 8 (2015) 702–730.

https://doi.org/10.1039/C4EE03229B.

[23] X. Lang, A. Hirata, T. Fujita, M. Chen, Nanoporous metal/oxide hybrid electrodes for electrochemical supercapacitors, Nat Nano. 6 (2011) 232–236. http://dx.doi.org/10.1038/nnano.2011.13.

[24] Z. Yu, J. Thomas, Energy storing electrical cables: Integrating energy storage and electrical conduction, Adv. Mater. 26 (2014) 4279–4285. https://doi.org/10.1002/adma.201400440.

[25] M.-J. Deng, P.-J. Ho, C.-Z. Song, S.-A. Chen, J.-F. Lee, J.-M. Chen, K.-T. Lu, Fabrication of Mn/Mn oxide core-shell electrodes with three-dimensionally ordered macroporous structures for high-capacitance supercapacitors, Energy Environ. Sci. 6 (2013) 2178–2185. https://doi.org/10.1039/C3EE40598B.

[26] H. Zhu, Q. Liu, J. Liu, R. Li, H. Zhang, S. Hu, Z. Li, Construction of Porous Hierarchical Manganese Dioxide on Exfoliated Titanium Dioxide Nanosheets as a Novel Electrode for Supercapacitors, Electrochim. Acta. 178 (2015) 758–766. https://doi.org/10.1016/j.electacta.2015.08.073.

[27] Y. Zhang, J. Li, F. Kang, F. Gao, X. Wang, Fabrication and electrochemical characterization of two-dimensional ordered nanoporous manganese oxide for supercapacitor applications, Int. J. Hydrogen Energy. 37 (2012) 860–866. https://doi.org/10.1016/j.ijhydene.2011.04.034.

[28] M. Shie, D.C. Chen, C. Wang, T. Chiang, S. Ding, Immersion behavior of gelatin-containing calcium phosphate cement, 4 (2008) 646–655. https://doi.org/10.1016/j.actbio.2007.10.011.

[29] H. Wang, C. Peng, F. Peng, H. Yu, J. Yang, Facile synthesis of MnO_2/CNT nanocomposite and its electrochemical performance for supercapacitors, Mater.

Sci. Eng. B. 176 (2011) 1073–1078. https://doi.org/https://doi.org/10.1016/j.mseb.2011.05.043.

[30] W. Cui, E. Beniash, E. Gawalt, Z. Xu, C. Sfeir, Biomimetic coating of magnesium alloy for enhanced corrosion resistance and calcium phosphate deposition, Acta Biomater. 9 (2013) 8650–8659. https://doi.org/10.1016/j.actbio.2013.06.031.

[31] J. Yan, Z. Fan, T. Wei, Z. Qie, S. Wang, M. Zhang, Preparation and electrochemical characteristics of manganese dioxide/graphite nanoplatelet composites, Mater. Sci. Eng. B. 151 (2008) 174–178. https://doi.org/https://doi.org/10.1016/j.mseb.2008.05.018.

[32] X. Wang, L. Liu, X. Wang, L. Yi, C. Hu, X. Zhang, Mn_2O_3/carbon aerogel microbead composites synthesized by in situ coating method for supercapacitors, Mater. Sci. Eng. B. 176 (2011) 1232–1238. https://doi.org/https://doi.org/10.1016/j.mseb.2011.07.003.

[33] P.K. Nayak, N. Munichandraiah, Rapid sonochemical synthesis of mesoporous MnO_2 for supercapacitor applications, Mater. Sci. Eng. B. 177 (2012) 849–854. https://doi.org/https://doi.org/10.1016/j.mseb.2012.04.004.

[34] H. Li, L. Deng, G. Zhu, L. Kang, Z.-H. Liu, Fabrication and capacitance of Ni^{2+}–Fe^{3+} LDHs/MnO_2 layered nanocomposite via an exfoliation/reassembling process, Mater. Sci. Eng. B. 177 (2012) 8–13. https://doi.org/https://doi.org/10.1016/j.mseb.2011.09.012.

[35] Y. Huang, J. Lu, S. Kang, D. Weng, L. Han, Y. Wang, Synthesis and application of MnO_2/PANI/MWCNT ternary nanocomposite as an electrode material for supercapacitors, Int. J. Electrochem. Sci. 14 (2019) 9298–9310.

https://doi.org/10.20964/2019.09.86.

[36] F. Yang, M. Xu, S.-J. Bao, Q.-Q. Sun, MnO_2-assisted fabrication of PANI/MWCNT composite and its application as a supercapacitor, RSC Adv. 4 (2014) 33569–33573. https://doi.org/10.1039/C4RA04905E.

[37] K. Li, X. Liu, T. Zheng, D. Jiang, Z. Zhou, C. Liu, X. Zhang, Y. Zhang, D. Losic, Tuning MnO_2 to FeOOH replicas with bio-template 3D morphology as electrodes for high performance asymmetric supercapacitors, Chem. Eng. J. 370 (2019) 136–147. https://doi.org/https://doi.org/10.1016/j.cej.2019.03.190.

[38] M.M. Sk, C.Y. Yue, K. Ghosh, R.K. Jena, Review on advances in porous nanostructured nickel oxides and their composite electrodes for high-performance supercapacitors, J. Power Sources. 308 (2016) 121–140. https://doi.org/10.1016/j.jpowsour.2016.01.056.

[39] X. Sun, Q. Li, Y. Lü, Y. Mao, Three-dimensional ZnO@MnO_2 core@shell nanostructures for electrochemical energy storage., Chem. Commun. (Camb). 49 (2013) 4456–8. https://doi.org/10.1039/c3cc41048j.

[40] X. Zhou, L. Ma, MnO_2/ZnO porous film: Electrochemical synthesis and enhanced supercapacitor performances, Thin Solid Films. 597 (2015) 44–49. https://doi.org/10.1016/j.tsf.2015.11.032.

[41] Z. Lei, J. Zhang, X.S. Zhao, Ultrathin MnO_2 nanofibers grown on graphitic carbon spheres as high-performance asymmetric supercapacitor electrodes, J. Mater. Chem. 22 (2012) 153–160. https://doi.org/10.1039/C1JM13872C.

[42] X. Zhang, X. Sun, H. Zhang, D. Zhang, Y. Ma, Microwave-assisted reflux rapid synthesis of MnO_2 nanostructures and their application in supercapacitors, Electrochim. Acta. 87 (2013) 637–644.

https://doi.org/https://doi.org/10.1016/j.electacta.2012.10.022.

[43] K. Li, S. Feng, C. Jing, Y. Chen, X. Liu, Y. Zhang, L. Zhou, Assembling a double shell on a diatomite skeleton ternary complex with conductive polypyrrole for the enhancement of supercapacitors, Chem. Commun. 55 (2019) 13773–13776. https://doi.org/10.1039/C9CC06791D.

[44] Z. Yu, B. Duong, D. Abbitt, J. Thomas, Highly ordered MnO_2 nanopillars for enhanced supercapacitor performance, Adv. Mater. 25 (2013) 3302–3306. https://doi.org/10.1002/adma.201300572.

[45] X. Liu, H. Zhang, J. Wang, Z. Wang, S. Wang, Preparation of epoxy microcapsule based self-healing coatings and their behavior, Surf. Coatings Technol. 206 (2012) 4976–4980. https://doi.org/https://doi.org/10.1016/j.surfcoat.2012.05.133.

[46] J. Liu, J. Jiang, C. Cheng, H. Li, J. Zhang, H. Gong, H.J. Fan, Co_3O_4 nanowire@MnO_2 ultrathin nanosheet core/shell arrays: A new class of high-performance pseudocapacitive materials, Adv. Mater. 23 (2011) 2076–2081. https://doi.org/10.1002/adma.201100058.

[47] B. Duong, Z. Yu, P. Gangopadhyay, S. Seraphin, N. Peyghambarian, J. Thomas, High Throughput Printing of Nanostructured Carbon Electrodes for Supercapacitors, Adv. Mater. Interfaces. 1 (2013) 1300014. https://doi.org/10.1002/admi.201300014.

[48] X. Lu, Y. Zeng, M. Yu, T. Zhai, C. Liang, S. Xie, M.-S. Balogun, Y. Tong, Oxygen-Deficient Hematite Nanorods as High-Performance and Novel Negative Electrodes for Flexible Asymmetric Supercapacitors, Adv. Mater. 26 (2014) 3148–3155. https://doi.org/10.1002/adma.201305851.

[49] G.-Y. Zhao, H.-L. Li, Preparation of polyaniline nanowire arrayed electrodes for electrochemical supercapacitors, Microporous Mesoporous Mater. 110 (2008) 590–594. https://doi.org/https://doi.org/10.1016/j.micromeso.2007.06.023.

[50] R.K. Sharma, A. Karakoti, S. Seal, L. Zhai, Multiwall carbon nanotube-poly(4-styrenesulfonic acid) supported polypyrrole/manganese oxide nano-composites for high performance electrochemical electrodes, J. Power Sources. 195 (2010) 1256–1262. https://doi.org/https://doi.org/10.1016/j.jpowsour.2009.08.093.

[51] X. Wang, J. Ding, S. Yao, X. Wu, Q. Feng, Z. Wang, B. Geng, High supercapacitor and adsorption behaviors of flower-like MoS_2 nanostructures, J. Mater. Chem. A. 2 (2014) 15958–15963. https://doi.org/10.1039/C4TA03044C.

[52] J. Feng, X. Sun, C. Wu, L. Peng, C. Lin, S. Hu, J. Yang, Y. Xie, Metallic Few-Layered VS_2 Ultrathin Nanosheets: High Two-Dimensional Conductivity for In-Plane Supercapacitors, J. Am. Chem. Soc. 133 (2011) 17832–17838. https://doi.org/10.1021/ja207176c.

[53] W. Liu, M. Zhu, J. Liu, X. Li, J. Liu, Flexible asymmetric supercapacitor with high energy density based on optimized MnO_2 cathode and Fe_2O_3 anode, Chinese Chem. Lett. 30 (2019) 750–756. https://doi.org/https://doi.org/10.1016/j.cclet.2018.09.013.

[54] X. Zhang, P. Yu, H. Zhang, D. Zhang, X. Sun, Y. Ma, Rapid hydrothermal synthesis of hierarchical nanostructures assembled from ultrathin birnessite-type MnO_2 nanosheets for supercapacitor applications, Electrochim. Acta. 89 (2013) 523–529. https://doi.org/https://doi.org/10.1016/j.electacta.2012.11.089.

[55] X. Zhang, X. Sun, H. Zhang, C. Li, Y. Ma, Comparative performance of birnessite-type MnO_2 nanoplates and octahedral molecular sieve (OMS-5)

nanobelts of manganese dioxide as electrode materials for supercapacitor, Electrochim. Acta 132 (2014) 315.

[56] B. Singu, K. Ro Yoon, Synthesis and characterization of MnO_2-decorated graphene for supercapacitors, 2017. https://doi.org/10.1016/j.electacta.2017.01.182.

[57] M. Yang, B. Choi, Rapid one-step synthesis of conductive and porous MnO_2/graphene nanocomposite for high performance supercapacitors, 2016. https://doi.org/10.1016/j.jelechem.2016.07.013.

[58] L. Lyu, K. Seong, J.M. Kim, W. Zhang, X. Jin, D.K. Kim, Y. Jeon, J. Kang, Y. Piao, CNT/High Mass Loading MnO_2/Graphene-Grafted Carbon Cloth Electrodes for High-Energy Asymmetric Supercapacitors, Nano-Micro Lett. 11 (2019) 88. https://doi.org/10.1007/s40820-019-0316-7.

[59] J. Shin, D. Shin, H. Hwang, T. Yeo, S. Park, W. Choi, One-step transformation of MnO_2 into MnO_2−x@carbon nanostructures for high-performance supercapacitors using structure-guided combustion waves, J. Mater. Chem. A. 5 (2017) 13488–13498. https://doi.org/10.1039/C7TA03259E.

[60] M. Ramadan, A.M. Abdellah, S.G. Mohamed, N.K. Allam, 3D Interconnected Binder-Free Electrospun MnO@C Nanofibers for Supercapacitor Devices, Sci. Rep. 8 (2018) 7988. https://doi.org/10.1038/s41598-018-26370-z.

[61] F.M. Ismail, M. Ramadan, A.M. Abdellah, I. Ismail, N.K. Allam, Mesoporous spinel manganese zinc ferrite for high-performance supercapacitors, J. Electroanal. Chem. 817 (2018) 111–117. https://doi.org/https://doi.org/10.1016/j.jelechem.2018.04.002.

[62] M. Pang, G. Long, S. Jiang, Y. Ji, W. Han, B. Wang, X. Liu, Y. Xi, One pot low-

temperature growth of hierarchical δ-MnO_2 nanosheets on nickel foam for supercapacitor applications, Electrochim. Acta. 161 (2015) 297–304. https://doi.org/https://doi.org/10.1016/j.electacta.2015.02.089.

[63] M. Cakici, R.R. Kakarla, F. Alonso-Marroquin, Advanced electrochemical energy storage supercapacitors based on the flexible carbon fiber fabric-coated with uniform coral-like MnO_2 structured electrodes, Chem. Eng. J. 309 (2017) 151–158. https://doi.org/https://doi.org/10.1016/j.cej.2016.10.012.

[64] J. Garcia-Torres, A.J. Roberts, R.C.T. Slade, C. Crean, One-step wet-spinning process of CB/CNT/MnO_2 nanotubes hybrid flexible fibres as electrodes for wearable supercapacitors, Electrochim. Acta. 296 (2019) 481–490. https://doi.org/https://doi.org/10.1016/j.electacta.2018.10.201.

[65] Y. Wang, X. Li, Y. Wang, Y. Liu, Y. Bai, R. Liu, G. Yuan, High-performance flexible MnO_2@carbonized cotton textile electrodes for enlarged operating potential window symmetrical supercapacitors, Electrochim. Acta. 299 (2019) 12–18. https://doi.org/https://doi.org/10.1016/j.electacta.2018.12.181.

[66] Y. Wang, W. Zhou, Q. Kang, J. Chen, Y. Li, X. Feng, D. Wang, Y. Ma, W. Huang, Patterning Islandlike MnO_2 Arrays by Breath-Figure Templates for Flexible Transparent Supercapacitors, ACS Appl. Mater. Interfaces. 10 (2018) 27001–27008. https://doi.org/10.1021/acsami.8b06710.

[67] A. Yabuki, S. Tanaka, Electrically conductive copper film prepared at low temperature by thermal decomposition of copper amine complexes with various amines, Mater. Res. Bull. 47 (2012) 4107–4111. https://doi.org/10.1016/j.materresbull.2012.08.052.

[68] A. Yabuki, N. Arriffin, M. Yanase, Low-temperature synthesis of copper

conductive film by thermal decomposition of copper–amine complexes, Thin Solid Films. 519 (2011) 6530–6533. https://doi.org/10.1016/j.tsf.2011.04.112.

[69] A. Yabuki, Y. Tachibana, I.W. Fathona, Synthesis of copper conductive film by low-temperature thermal decomposition of copper-aminediol complexes under an air atmosphere, Mater. Chem. Phys. 148 (2014) 299–304. https://doi.org/10.1016/j.matchemphys.2014.07.047.

[70] T. Brousse, D. Belanger, J.W. Long, To Be or Not To Be Pseudocapacitive?, J. Electrochem. Soc. 162 (2015) A5185–A5189. https://doi.org/10.1149/2.0201505jes.

[71] G. Fregonara, S. Trasatti, Inner and Outer Active Surface Electrodes, (1989) 5–9. https://doi.org/http://dx.doi.org/10.1016/0013-4686(90)85068-X.

[72] W.-C. Chen, T.-C. Wen, H. Teng, Polyaniline-deposited porous carbon electrode for supercapacitor, Electrochim. Acta. 48 (2003) 641–649. https://doi.org/https://doi.org/10.1016/S0013-4686(02)00734-X.

[73] F. Rafik, H. Gualous, R. Gallay, A. Crausaz, A. Berthon, Frequency, thermal and voltage supercapacitor characterization and modeling, J. Power Sources. 165 (2007) 928–934. https://doi.org/https://doi.org/10.1016/j.jpowsour.2006.12.021.

[74] Y.-R. Nian, H. Teng, Influence of surface oxides on the impedance behavior of carbon-based electrochemical capacitors, J. Electroanal. Chem. 540 (2003) 119–127. https://doi.org/https://doi.org/10.1016/S0022-0728(02)01299-8.

[75] J. Gamby, P.L. Taberna, P. Simon, J.F. Fauvarque, M. Chesneau, Studies and characterisations of various activated carbons used for carbon/carbon supercapacitors, J. Power Sources. 101 (2001) 109–116. https://doi.org/https://doi.org/10.1016/S0378-7753(01)00707-8.

[76] I.W. Fathona, A. Yabuki, Mesh-like thin-film electrodes of manganese oxide with high specific capacitance synthesized via thermal decomposition of manganese formate-amine complexed ink, Mater. Res. Bull. 112 (2019) 346–353. https://doi.org/https://doi.org/10.1016/j.materresbull.2019.01.004.

Figure captions

Fig.1. Thermal gravimetric analysis of (a) Mnf, (b) Mnf-heptylamine-hexanol, (c) Mnf-octylamine-hexanol, and (d) Mnf-nonylamine-hexanol inks under air. The molar ratio of Mnf:amine:hexanol was 1:2:0.5.

Fig. 2. Cyclic voltammetry of a thin-film electrode fabricated from Mnf-octylamine-hexanol ink at a molar ratio of 1:2:0.5 at 180 ºC. The scan rate was 50 mV s^{-1}.

Fig. 3. Specific capacitance calculated from CV curves of thin-film electrodes fabricated at 180 ºC from (a) Mnf-heptylamine-hexanol, (b) Mnf-octylamine-hexanol, and (c) Mnf-nonylamine-hexanol inks. The molar ratio of Mnf:amine:hexanol was 1:2:0.5. The scan rate was 50 mV s^{-1}.

Fig. 4. CV curves of the thin-film electrodes fabricated at 180 ºC from Mnf-octylamine-hexanol inks with Mnf:octylamine ratios of (a) 1:1, (b) 1:2, (c) 1:3, and (d) 1:4. The scan rate was 50 mV s^{-1}.

Fig. 5. Specific capacitance calculated from the CV curves of the thin-film electrodes fabricated at 180 ºC from Mnf-octylamine-hexanol inks with Mnf:octylamine ratios of (a) 1:1, (b) 1:2, (c) 1:3, and (d) 1:4. The scan rate was 50 mV s^{-1}.

Fig. 6. Specific capacitance calculated from the CV curves after 50 cycles for a thin-film electrode fabricated from Mnf-octylamine-hexanol ink with Mnf:octylamine ratios

of (a) 1:1, (b) 1:2, (c) 1:3, and (d) 1:4 at various temperatures. The scan rate was 50 mV s^{-1}.

Fig. 7. Specific capacitance calculated from the CV curves after 50 cycles of a thin-film electrode fabricated from Mnf-octylamine-hexanol ink with a Mnf:octylamine ratio of 1:3 at various scan rates.

Fig. 8. Charge-discharge curves during 48 to 50 cycles of thin-film electrodes fabricated at 180 ^{o}C from Mnf-octylamine-hexanol ink with a Mnf:amine ratio of 1:3 at 1 mA (a) and 10 mA (b).

Fig. 9. Nyquist plot of a thin-film electrode fabricated at 180 ^{o}C from Mnf-octylamine-hexanol ink with a Mnf:amine ratio of 1:3.

Fig. 10. Specific capacitances of thin-film electrodes fabricated from Mnf-octylamine-hexanol ink with Mnf:amine molar ratios of 1:3 at 180 ^{o}C calculated from CV during 1,000 cycles at a scan rate 50 mV s^{-1}.

Fig. 11. Surface morphology of thin films fabricated at 180 ^{o}C from Mnf-octylamine-hexanol ink with Mnf:amine ratios of (a) 1:2, (b) 1:3, and (c) 1:4 after 50 cycles of CV measurement with a scan rate of 50 mV s^{-1}.

Fig. 12. Surface morphology of thin films fabricated at (a) 170 ºC, and (b) 210 ºC from Mnf-octylamine-hexanol ink with a Mnf:amine ratio of 1:3 after 50 cycles of CV measurement with a scan rate of 50 mV s^{-1}.

Fig. 13. Surface morphology of a thin film fabricated at 180 ºC from Mnf-octylamine-hexanol ink with a Mnf:amine ratio of 1:3 before electrochemical measurement.

Fig. 14. XRD pattern of thin-film electrodes fabricated at 180 ºC from Mnf-octylamine-hexanol ink with a Mnf:amine molar ratio of 1:3 (a) before and (b) after immersion in an electrolyte solution, and ink with a ratio of 1:2 before immersion in electrolyte (c).

Fig.15. Mechanism of the formation and growth of a thin-film electrode with high specific capacitance through calcination and electrochemical measurement in an electrolyte solution to generate an electrochemically active surface.